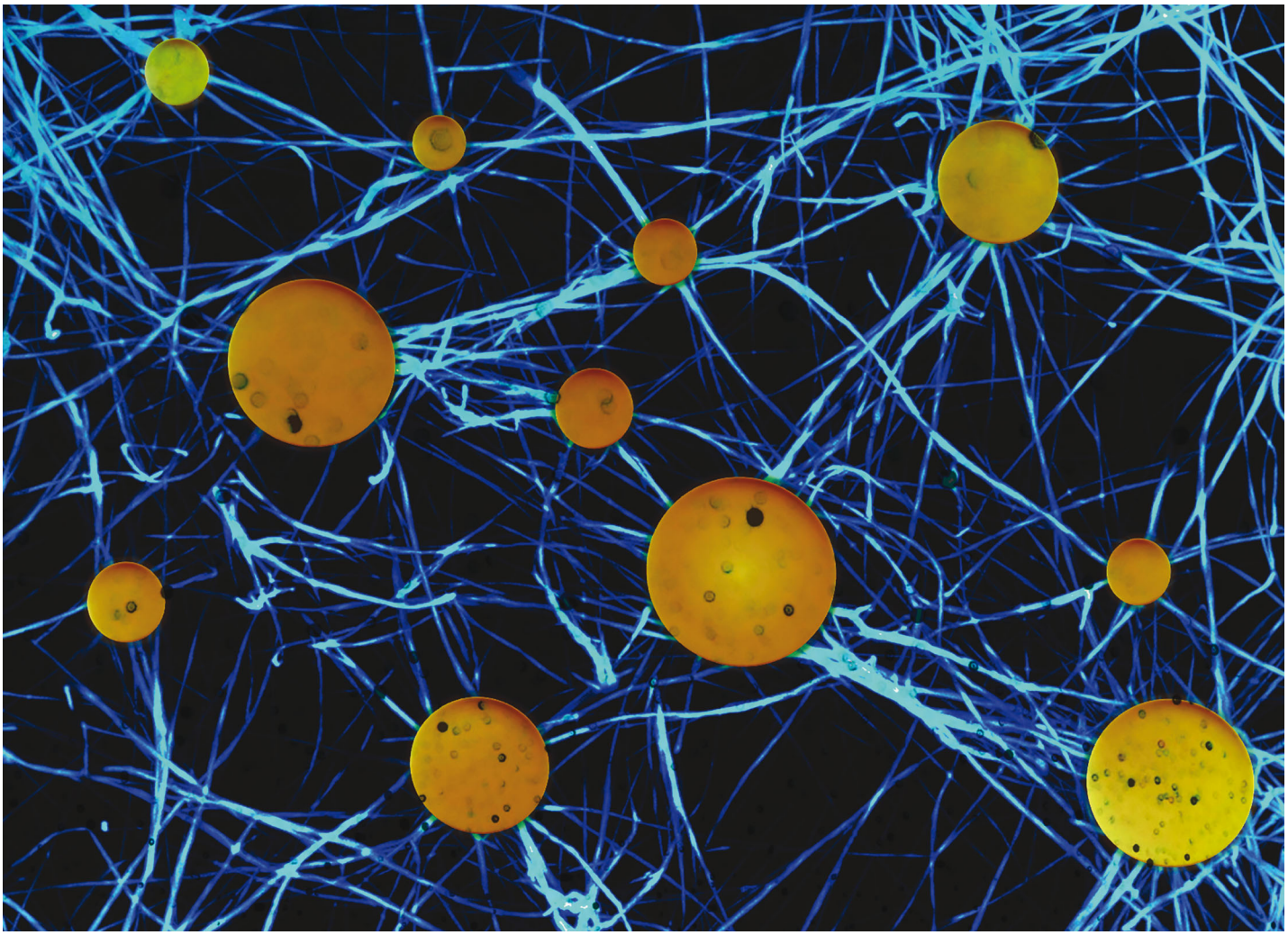

Highlighting the collaborative research from the groups of Prof. Wenxiang Xu (Hohai University), Prof. Bo Sun (Oregon State University) and Prof. Yang Jiao (Arizona State University)
Active contractile particles on random network mimicking migrating cells in 3D Extracellular Matrix (ECM)

Absorbing–active transition in a multi-cellular system regulated by a dynamic force network

Migrating cells in 3D can generate active pulling forces, which lead to a dynamically evolving force network in the system. We elucidate the role of such force network in regulating collective cell behaviors using an active-particle-on-network (APN) model, in which active particles can pull the fibers and hop between neighboring nodes of the network following local durotaxis. Our model reveals interesting collective cellular dynamics regulated by the force network.

As featured in:

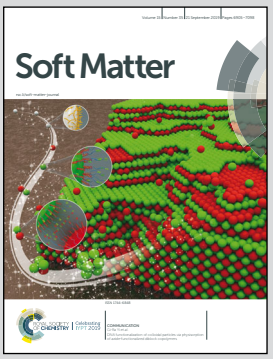

See Wenxiang Xu, Bo Sun, Yang Jiao *et al.*, *Soft Matter*, 2019, **15**, 6938.

ROYAL SOCIETY OF CHEMISTRY | Celebrating IYPT 2019

rsc.li/soft-matter-journal

Registered charity number: 207890

Soft Matter

PAPER

View Article Online
View Journal | View Issue

Cite this: *Soft Matter*, 2019, 15, 6938

Absorbing–active transition in a multi-cellular system regulated by a dynamic force network†

Hanqing Nan,[a] Yu Zheng,[b] Yiheng H. Lin,[ac] Shaohua Chen,[d] Christopher Z. Eddy,[e] Jianxiang Tian,[af] Wenxiang Xu,*[ag] Bo Sun*[e] and Yang Jiao*[ab]

Received 21st June 2019,
Accepted 2nd August 2019

DOI: 10.1039/c9sm01244c

rsc.li/soft-matter-journal

Collective cell migration in 3D extracellular matrix (ECM) is crucial to many physiological and pathological processes. Migrating cells can generate active pulling forces *via* actin filament contraction, which are transmitted to the ECM fibers and lead to a dynamically evolving force network in the system. Here, we elucidate the role of this force network in regulating collective cell behaviors using a minimal active-particle-on-network (APN) model, in which active particles can pull the fibers and hop between neighboring nodes of the network following local durotaxis. Our model reveals a dynamic transition as the particle number density approaches a critical value, from an "absorbing" state containing isolated stationary small particle clusters, to an "active" state containing a single large cluster undergoing constant dynamic reorganization. This reorganization is dominated by a subset of highly dynamic "radical" particles in the cluster, whose number also exhibits a transition at the same critical density. The transition is underlaid by the percolation of "influence spheres" due to the particle pulling forces. Our results suggest a robust mechanism based on ECM-mediated mechanical coupling for collective cell behaviors in 3D ECM.

I. Introduction

Collective cell migration is crucial to many physiological and pathological processes such as tissue regeneration, immune response and cancer progression.[1–4] Cell migration in 3D extracellular matrix (ECM) is a complex dynamic process involving a series of intra-cellular and extra-cellular activities,[5,6] and it can be regulated by a variety of cell–ECM interactions *via* chemotaxis,[7] durotaxis,[8–10] haptotaxis,[11] and contact guidance.[12–14] A migrating cell also generates active pulling forces, which are transmitted to the ECM fibers *via* focal adhesion complexes[15,16] and consistently remodel the local ECM (*e.g.*, by re-orienting the collagen fibers, forming fiber bundles and increasing the local stiffness of the ECM).[17–24] In a multi-cell system, the pulling forces generated by individual cells can give rise to a dynamically evolving force network (carried by the ECM fibers).[25,29] The force network can further influence the migration of the cells, which in turn alters the ECM and the force network.[26–33] This feedback loop between the force network and cell migration could lead to a rich spectrum of collective migratory behaviors.

The cell–ECM system is an example of a complex many-body system in which the individuals (*e.g.*, migrating cells) communicate and interact with one another through their environment (*e.g.*, ECM), while simultaneously re-shaping the environment, altering the means (*e.g.*, the force network) to pass information among themselves. Other examples of such complex systems include flocks of birds, schools of fish, and active swimmers in a crowded environment.[34,35] In these systems, although there are no physical force networks as in the cell–ECM system, the communications between the near neighbors effectively establish a certain "information network", which passes important signals among the individuals in the system and regulates their collective behaviors. For example, it was recently shown that chemotactic interaction networks in active suspensions can lead to novel collective behaviors (from clustering to moving in stable ordered groups).[36]

In this paper, we investigate the collective cellular dynamics and self-organizing multi-cellular patterns in 3D ECM resulting from the dynamically evolving force network, using a minimal active-particle-on-network (APN) model. Although focusing on the cell–ECM system, the physical insights obtained here are also valuable to understanding active-particle systems dominated by environment-mediated particle–particle interactions.

[a] *Materials Science and Engineering, Arizona State University, Tempe, AZ 85287, USA. E-mail: yang.jiao.2@asu.edu*
[b] *Department of Physics, Arizona State University, Tempe, AZ 85287, USA*
[c] *Shenzhen Middle School, Shenzhen 518001, P. R. China*
[d] *Department of Materials Engineering, KU Leuven, Kasteelpark Arenberg 44 Bus 2450, Leuven, Belgium*
[e] *Department of Physics, Oregon State University, Corvallis, OR 97331, USA. E-mail: sunb@onid.orst.edu*
[f] *Department of Physics, Qufu Normal University, Qufu 273165, P. R. China*
[g] *College of Mechanics and Materials, Hohai University, Nanjing 211100, P. R. China. E-mail: xwxfat@gmail.com*

† Electronic supplementary information (ESI) available. See DOI: 10.1039/c9sm01244c

II. Results

A. Active-particle-on-network model

We now describe our active-particle-on-network (APN) model: The 3D ECM is modeled as a discrete network with a "graph" (*i.e.*, node-bond) representation in a cubic simulation domain with linear size L, which is composed of M_n nodes and M_b bonds. The average coordination number Z, *i.e.*, the average number of bonds connected to each node, is given by $Z = 2M_b/M_n$. We have used both the periodic boundary (PB) conditions and fixed boundary (FB) conditions (*i.e.*, the nodes within a certain distance δL from the boundaries of the simulation domain are fixed) in our simulations, and we find that even for a moderate system size (*e.g.*, $M_n \sim 5000$), the boundary conditions do not affect the results. In the subsequent discussions, we will mainly present the results obtained using the fixed boundary conditions, under which M_n denotes the number of free (non-fixed) nodes.

Next, N_p active particles (*e.g.*, congruent spheres) are introduced into the network such that each particle occupies a randomly selected un-occupied node (*i.e.*, each node can be occupied by only one particle). The number density ρ of the particles is defined as $\rho = N_p/M_n$, *i.e.*, the fraction of nodes occupied by the active particles. Each particle can generate a contraction, which pulls all of the bonds connected to the node it occupies towards the particle center (*i.e.*, the node) by a fixed amount δl, leading to different pulling forces in the bonds and thus, a force network in the system. We consider that the particles can "migrate" from their original node to an un-occupied neighboring node following local durotaxis, *i.e.*, along the bond with the highest stiffness, which is also the bond that carries the largest pulling force among all neighboring bonds (see Fig. 1a for illustration). The diameter of the particles is not essential in our model and thus, it is not explicitly considered here.

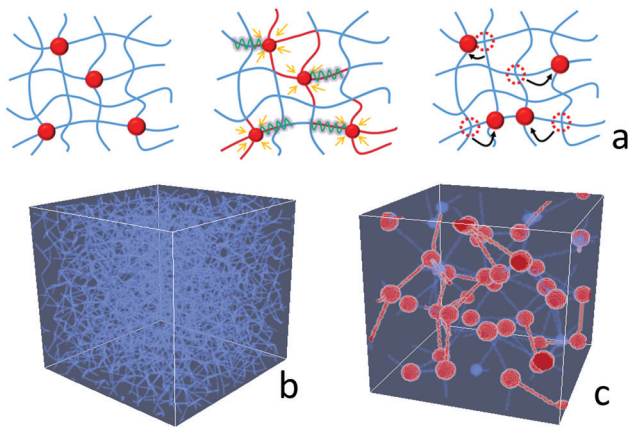

Fig. 1 (a) Schematic illustration of the active-particle-on-network (APN) model. Left: Particles on a stress-free network. Middle: Particle contraction leads to a "force network" composed of high-stress fibers (illustrated using red). Right: Particles migrating on the ECM network along fibers carrying the largest forces. (b) 3D visualization of a random network derived from a random jammed packing of hard spheres. (c) Force network (carried by the high-stress fibers highlighted using a red color) generated by contractile particles (shown as red spheres) on the network. For better visualization, only a small sub-network is shown here.

The bonds of the network are modeled as elastic elements with only a non-zero stretching modulus E_s and they are free to rotate at the nodes. An active particle can generate pulling forces in the bonds connected to the node it occupies by contraction, *i.e.*, δl. This contraction leads to a strain $\varepsilon_i = \delta l/l_i$ in the bond i with an original length l_i, and thus, a pulling force $f_s = E_s A \delta l/l_i$, where A is an effective cross-sectional area of the bonds. These pulling forces impose force boundary conditions for the ECM network, and the force-balance network configuration is obtained using an iterative force-based relaxation approach.[32]

We note that many factors can affect the interactions between the dynamic force network and the collective dynamics of the active particles in our APN model. These may include the geometry/topology and mechanical properties of the network, as well as the number density, spatial distribution and the contractibility (*i.e.*, δl) of the active particles. In this work, we mainly focus on disordered isostatic networks (*i.e.*, $Z = 6$) derived from maximally random jammed packings of congruent hard spheres,[37,38] see Fig. 1b. It is straightforward to generalize this study to random network models derived from confocal images of collagen gels[39,40] or ordered networks, which we will investigate later. In addition, we use simple linear elastic network models. This allows us to investigate the system in the elastic regime,[41] in which the force network is mainly determined by the number density and spatial distribution of the active particles, and largely independent of particle contractibility. Our model can readily incorporate more realistic mechanical models for the ECM, taking into account non-linear responses of the fibers[42,43] and plasticity.[22] Moreover, in an actual cell–ECM system, the cell migration might not be sensitive to individual stiffer fibers, but determined by certain meso-scale stiff structures emerging due to cell remodeling, such as bundles of high-stress fibers. Nonetheless, we believe that the general organizational principles of active particles on random networks obtained here are relevant to and can provide insights on actual cell–ECM systems.

B. Density-induced absorbing–active transition

We now describe the observed collective dynamics of the active particles on the random networks. In our simulations, we systematically vary the particle number density $\rho \in (0.05,0.95)$. For each ρ, the particles are initially randomly introduced in the network and the system is allowed to evolve according to the aforementioned APN dynamics. At low densities (*i.e.*, $\rho < \rho_c \approx 0.114$), the particles rapidly aggregate into multiple isolated small clusters, which are randomly distributed within the ECM (see Fig. 2a and b). Here, we consider that two particles belong to the same "cluster" if they occupy two nodes connected by the same bond. As ρ approaches ρ_c from below, the maximal cluster size n_c (*i.e.*, the number of particles in the largest cluster of the system) increases dramatically (see Fig. 2c), indicating that the majority of the particles are connected to form a single large cluster in the system.

In addition, we find that the isolated small clusters associated with $\rho < \rho_c$ are stationary, *i.e.*, the particles in the clusters either do not move at all or hop between two adjacent nodes (typically at the boundary of a cluster). On the other hand, the dominant

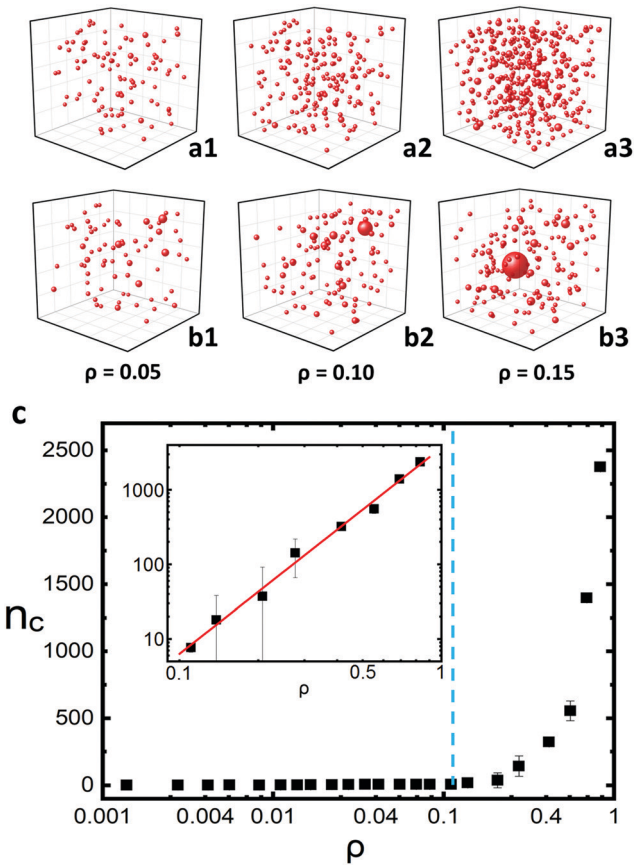

Fig. 2 (a) Initial distribution of clusters formed by randomly placed active particles on the network for different number density ρ. In these plots, a cluster is represented by a sphere for better visualization with the center coinciding with the center of the cluster and the radius representing the cluster size. (b) Distribution of clusters in the final state of the APN system. As ρ increases, the majority of particles tend to aggregate into a single large cluster in the system. (c) The maximal cluster size n_c (see definition in the text) as a function of ρ. A transition behavior is apparent as ρ approaches $\rho_c \approx 0.114$ from below (indicated by the dashed line). The inset shows the log-scale plot of n_c for $\rho > \rho_c$. The statistics are obtained by averaging over 20 independent simulations.

large clusters formed for $\rho > \rho_c$ undergo constant dynamic reorganization. As illustrated in Fig. 3, for $\rho > \rho_c$, we observe that the dominant cluster in the system contains a subset of highly dynamic particles that are able to visit many distinct nodes for a given number of steps, while the remaining particles are in the local absorbing state, hopping between adjacent sites. We refer to these highly dynamic particles as "radicals", *i.e.*, those that do not possess a periodic hopping pattern over a finite number of nodes.

To further quantify the dynamics of the clusters, we count the number of distinct nodes m_s visited by a particle during a total of s successive steps. The collected statistics for different particle densities are shown in Fig. 4a. We note that the m_s statistics shown in Fig. 4a does not depend on s and we have used $s = 24$ here. It can be seen from Fig. 4a that for small ρ, a particle can only visit one or two nodes, respectively, indicating that the particle does not move or can only hop between two adjacent nodes. As ρ approaches ρ_c from below, although the

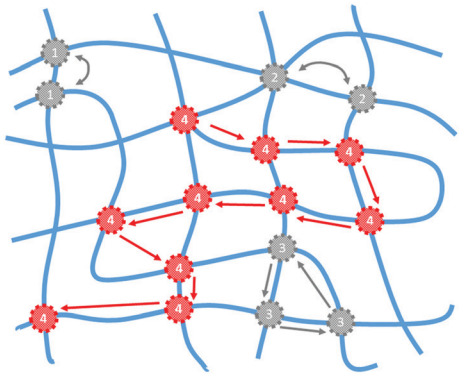

Fig. 3 Schematic illustration of a "radical" in the system. As ρ approaches ρ_c from below, a subset of highly dynamic particles (shown in red) emerge, which are able to visit many distinct nodes for a given number of steps and are referred to as "radicals". These radicals determine the dynamic re-organization of the dominant cluster in the system.

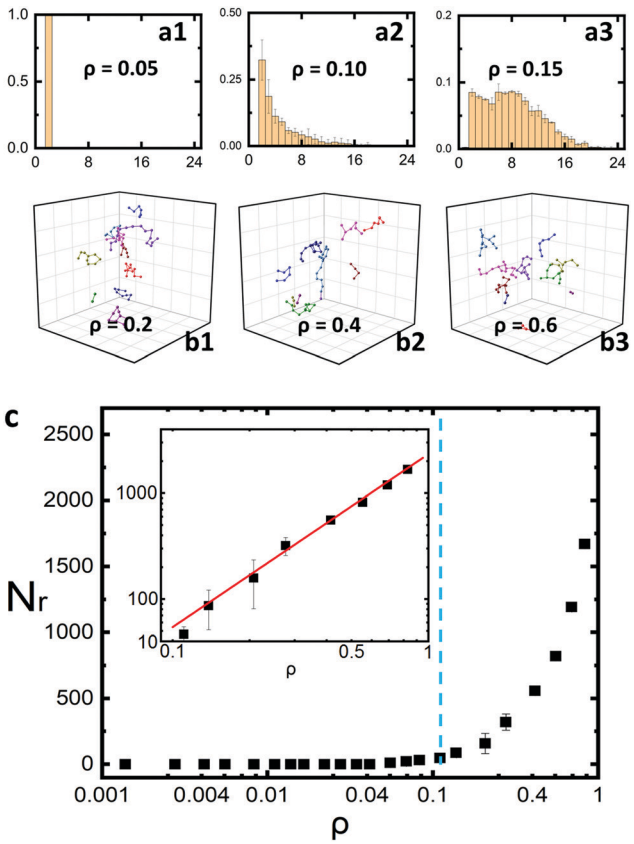

Fig. 4 (a) Statistics of the number of distinct nodes m_s visited by a particle for $s = 24$ successive steps for different number density ρ. The emergence of "radicals" is indicated by the emergence of the second peak associated with large node numbers in the m_s statistics. (b) Representative trajectories for 10 randomly selected radicals (*i.e.*, highly dynamic particles) for different ρ. (c) The number of radicals N_r as a function of ρ, which exhibits a clear transition at $\rho_c \approx 0.114$ (indicated by the dashed line). This is consistent with the transition observed in the maximal cluster size n_c as ρ increases (see Fig. 2c). The inset shows the log-scale plot of N_r for $\rho > \rho_c$.

majority of particles are localized (indicated by the peak in the m_s statistics associated with small node numbers), a subset of

highly dynamic particles (*i.e.*, the "radicals") emerge, which are able to visit many distinct nodes for a given number of steps (indicated by the emergence of the second peak associated with large node numbers in the m_s statistics). These highly dynamic "radicals" do not possess a periodic hopping pattern over a finite number of nodes. The trajectory of a small number of randomly selected radicals is shown in Fig. 4b for different ρ values. Fig. 4c shows the number of radicals N_r as a function of ρ. It can be seen that N_r exhibits a clear transition as ρ increases towards ρ_c. This is consistent with the transition observed in the maximal cluster size n_c as ρ increases (see Fig. 2c).

The above analysis suggests that the system possesses a phase-transition-like behavior, as the particle number density ρ increases, from an "absorbing" state in which the particles segregate into small isolated stationary clusters, to an "active" state, in which the majority of particles join in a single large dynamic cluster. This transition is also quantitatively manifested in the maximal cluster size $n_c(\rho)$ (Fig. 2c) and radial number $N_r(\rho)$ (Fig. 4c) as ρ increases towards $\rho_c \approx 0.114$. In particular, our scaling analysis shows that as ρ_c is approached from above, $n_c \sim (\rho - \rho_c)^{\alpha}$, where the critical exponent $\alpha \approx 6.6 \pm 0.1$. In addition, we find that $N_r \sim (\rho - \rho_c)^{\beta}$, where the critical exponent $\beta \approx 1.63 \pm 0.04$. The numerical values of α, β and ρ_c are obtained by fitting the simulation data. We also note that the ρ_c value is much lower than the site percolation threshold for the network (≈ 0.310).[44] The absorbing-to-active transition has also been observed in a wide spectrum of "random-organizing" physical systems, such as periodically driven colloids,[45–47] granular materials and amorphous solids,[48–50] vortices,[51] skyrmion systems[52] and hyperuniform fluids.[53] We will further elaborate the connections between the APN system and other random organizing systems in the Discussion section.

C. Mean field theory: percolation of influence sphere

We now investigate the mechanisms for the observed transition. Once a particle pulls the fibers, a stress gradient is built up surrounding this particle. When another particle "senses" the pulling force,[31] it will tend to move up the stress gradient towards the contracting particle due to local durotaxis. This would lead to an effective mutual pulling between the particles.

It is reasonable to assume that the pulling forces generated by a specific particle can only influence other particles within a certain distance R_I. Due to the intrinsic network heterogeneity, R_I may vary for different particles. Here, we take a "mean-field" approach and assign the same effective R_I to all the particles in the system and introduce the concept of the influence sphere, which is a spherical region with radius R_I centered at a contractile particle (see the inset of Fig. 5).

The influence-sphere radius R_I is estimated from the cluster statistics of the APN systems at low ρ, *i.e.*, those containing multiple small isolated stationary clusters in the final state. This is based on the assumption that at low ρ, only particles that are within the influence region of one another would eventually aggregate. In particular, we first identify the particles within the same cluster in the final state of the system. Then, the system is "re-winded" to the initial state, and the intra-cluster nearest-neighbor distance d_n is computed for all clusters. We then use the mean nearest-neighbor distance $\bar{d}_n$ to estimate $R_I \approx 0.104L$ (where L is the linear system size), which is roughly twice the average fiber length (see ESI† for fiber length distributions).

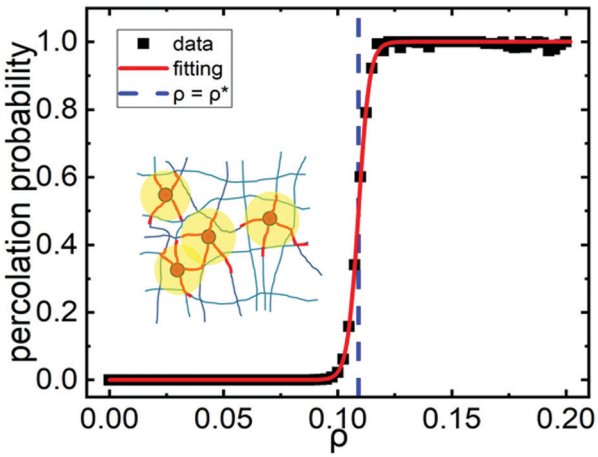

Fig. 5 Percolation probability analysis indicates a percolation transition of overlapping influence spheres with radius $R_I = 0.104L$ at $\rho^* \approx 0.109$, which agrees well with the critical density $\rho_c \approx 0.114$ for the dynamic phase transition in the APN system. Inset: Schematic illustration of the concept of the influence region (yellow circles), characterizing the range of the pulling forces (red) due to particle (red) contraction.

We now investigate the percolation of the influence spheres as ρ increases. For a given ρ, we randomly place particles on the ECM network. Instead of allowing the particles to move according to the APN dynamics, we place a virtual sphere with radius $R_I = 0.104L$ at each particle, representing the influence spheres. We subsequently identify the clusters formed by the influence spheres, based on which the percolation of the system can be determined.

Fig. 5 shows the percolation probability analysis for the system[54] (see ESI† for details), from which a percolation transition and the associated critical density (*i.e.*, percolation threshold) $\rho^* \approx 0.109$ can be clearly identified. Interestingly, the percolation transition of the influence spheres coincides with the absorbing–active transition of the active particles at $\rho_c \approx 0.114$. This suggests that the dynamic transition of the active particles from the "absorbing" state to the "active" state is underlaid by and can be understood as the percolation transition of the influence spheres.

In the aforementioned percolation model, we focused on the particles and employed a "mean-field" approximation for the force network, *i.e.*, by assigning an influence sphere to each particle. An alternative approach is to explicitly consider the dynamic force network. In this case, one can consider that the high-stress bonds can guide the migration of the particles (*i.e.*, the particles "flow" along such bonds). Therefore, if a connected pathway composed of such high-stress bonds is established and spans the entire system, the particles would be able to follow it and eventually aggregate into a single large cluster. This corresponds to a dynamic bond percolation problem, which was first introduced to study diffusion in a disordered

network in which the transition rates of the bonds of the network are dependent on time.[55]

In addition, it has been shown that in static elastic percolation networks, when the bonds carry only central tensile forces, the percolation threshold is higher than the connectivity threshold.[56] In our APN model, the influence spheres can possess a size that extends over several bond lengths. This effectively increases the connectivity, which results in the observed lower percolation threshold than that for the connectivity percolation. This is in contrast to the case of elastic percolation networks, in which the stressed bonds are a subset of all bonds.

III. Discussion

A. Effects of network geometry and topology on the absorbing–active transition

We also investigated the collective dynamics of active particles on other network models, including the networks derived from the diamond lattice, as well as random networks reconstructed based on confocal images (see ESI† for details). The same linear elastic bond model was employed for these networks, which allows us to focus on the effects of network geometry and topology on the collective behavior of the particle and the absorbing–active transition.

Fig. 6 shows the evolution of the maximal cluster size n_c as the particle number density ρ increases for the image-based random networks (IBRNs) (left panel) and diamond-lattice networks (DLNs) (right panel). It can be seen that both systems exhibit clear transition behaviors as observed in the packing-based random networks. In particular, the critical densities are respectively $\rho_c^{IBRN} \approx 0.28$ and $\rho_c^{DLN} \approx 0.12$. These values are also consistent with the estimates based on the statistics of the number of radicals N_r as a function of ρ and mean-field theory estimates (see ESI† for details). These results indicate that the absorbing–active transition is very robust and can occur on networks with different degrees of topological and geometrical order. This also suggests that a feedback loop between the evolving force network and particle dynamics provides a robust mechanism for regulating collective migratory behaviors.

We note that the transition density ρ_c depends on the network features. In particular, the system based on IBRNs possesses a significantly higher ρ_c than the other two systems. This is because the IBRN possesses a wide and heterogeneous distribution of bond lengths. As the particles generate active contraction, the shorter bonds carry larger tensile forces and thus, serve as local "attractors" (which effectively attract particles to the nodes they connect). Such local attractors can stabilize the isolated clusters, *i.e.*, the absorbing state, even at a relatively higher density.

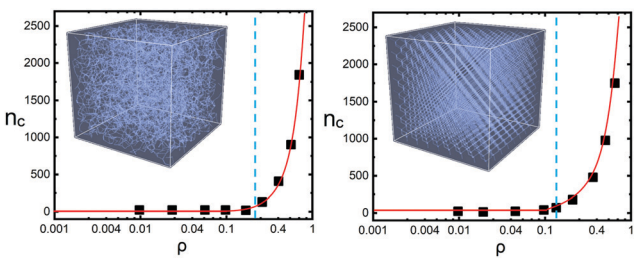

Fig. 6 The maximal cluster size n_c as a function of the particle number density ρ for the image-based random networks (IBRNs) (left) and diamond-lattice networks (DLNs) (right). The critical transition densities are respectively $\rho_c^{IBRN} \approx 0.28$ and $\rho_c^{DLN} \approx 0.12$. The insets show 3D visualizations of the network models.

B. Random organization in cell–ECM systems

As briefly mentioned above, the absorbing–active transitions have been observed in a wide class of systems characterized by random organization (RO). A canonical example of a RO system is periodically sheared colloidal suspension,[45] in which irreversible collisions can lead to a self-organized non-fluctuating quiescent (absorbing) state at low densities, with a dynamical phase transition separating it from fluctuating diffusing (active) states at high densities.

Our APN system is different from previous studied RO systems in the sense that the absorbing–active transition not only depends on fundamental characteristics of the particles (*e.g.*, number density, contractility, *etc.*) but also strongly depends on the micro-environment (*i.e.*, the geometry and topology of the ECM networks), which provides the scaffold to host the active force network regulating the collective dynamics of the particles. As discussed in the previous section, networks with strong attractors can stabilize absorbing states at relatively high density.

We note that although our results suggest that the absorbing–active transition in the APN system is continuous in nature, we could not completely exclude the possibility of a weak first-order transition here. Moreover, the two critical exponents, α and β, which respectively characterize the bulk growth of the particle aggregation and the increase of the number of highly dynamic radicals as the density passes the critical point, appear to be much larger than the ones typically found in percolation studies.[56,57] These two exponents do not have direct analogs in percolation studies, which usually focus on the emergence of overall rigidity, conductivity, and diverging length scale associated with the percolating cluster, *etc.* However, we can convert the bulk exponent α to a new exponent characterizing the linear size of the aggregation, *i.e.*, $\mu = \alpha/3 \approx 2.2$. Interestingly, the value of μ is very close to the critical exponent $f \approx 2.1$,[56] which characterizes the emergence of the overall elastic moduli of chemical gels dominated by central forces.

To verify the model predictions, we also designed *in vitro* experiments to investigate the collective dynamics of invasive MDA-MB-231 breast cancer cells in collagen gel.[58] In particular, the highly motile MDA-MB-231 cells were first co-cultured with non-metastatic MCF-7 cells at various densities with a 1 to 1 number ratio. The 2D substrate was then covered by a layer of collagen gel with 2 mg ml^{-1} concentration, which allows the invasive cells to migrate into the collagen. This design induces a strong polarization in the migration of the invasive cells (in the vertical direction), which allows us to clearly identify aggregation (clustering) of the cells in the lateral directions due to the dynamic force network. Interestingly, a clear density-dependent absorbing–active transition is observed in the experiments (see ESI†),

which suggests the validity of our model. The experimental details and results are reported elsewhere.[58]

IV. Conclusions

In summary, we have developed a novel APN model to investigate collective multi-cellular dynamics in a 3D ECM network, which is regulated by the dynamic force networks generated by active cell contraction. A novel type of absorbing–active transition has been discovered in the system, which depends on both the density of active particles (cells) and the topological and geometrical features of the ECM network. The critical transition density can be accurately estimated using a mean-field model considering the percolation of influence spheres associated with the range of active pulling forces generated by the contractile particles (cells).

Finally, we emphasize again that our minimal APN model does not take into account crucial mechanisms in actual cell migration such as ECM remodeling (*e.g.*, orientation, bundling and degradation) and cell–cell adhesion. Interestingly, our studies indicate that, at least for the APN systems, the local durotaxis for the active particles is sufficient to induce and stabilize aggregations, even without adhesion. Nonetheless, we expect that the insights on the collective behaviors of active particles regulated by the dynamically evolving force network obtained here are helpful in understanding the collective dynamics emerging in actual multi-cellular-ECM systems, as well as in other active-particle systems dominated by environment-mediated particle–particle interactions. In future work, we will also explore the effects of fiber alignment and external mechanical cues.

Conflicts of interest

There are no conflicts to declare.

Acknowledgements

H. N., Y. Z., and Y. J. thank Arizona State University for the generous start-up funds and the University Graduate Fellowship. W. X. was supported by the National Natural Science Foundation of China (Grant No. 11772120). C. E and B. S. are grateful for the support from the Scialog Program sponsored jointly by Research Corporation for Science Advancement and the Gordon and Betty Moore Foundation. B. S. is partially supported by the Medical Research Foundation of Oregon and SciRIS-II award from Oregon State University and by the National Science Foundation Grant PHY-1400968.

References

1 A. Aman and T. Piotrowski, Cell migration during morphogenesis, *Dev. Biol.*, 2010, **341**(1), 20–33.
2 P. Friedl and D. Gilmour, Collective cell migration in morphogenesis, regeneration and cancer, *Nat. Rev. Mol. Cell Biol.*, 2009, **10**(7), 445.
3 A. Vaezi, C. Bauer, V. Vasioukhin and E. Fuchs, Actin cable dynamics and Rho/Rock orchestrate a polarized cytoskeletal architecture in the early steps of assembling a stratified epithelium, *Dev. Cell*, 2002, **3**(3), 367–381.
4 S. Werner, T. Krieg and H. Smola, Keratinocyte-fibroblast interactions in wound healing, *J. Invest. Dermatol.*, 2007, **127**(5), 998–1008.
5 A. J. Ridley, M. A. Schwartz, K. Burridge, R. A. Firtel, M. H. Ginsberg, G. Borisy, J. T. Parsons and A. R. Horwitz, Cell migration: integrating signals from front to back, *Science*, 2003, **302**(5651), 1704–1709.
6 P. Friedl and E.-B. Bröcker, The biology of cell locomotion within three-dimensional extracellular matrix, *Cell. Mol. Life Sci.*, 2000, **57**(1), 41–64.
7 H. Szurmant and G. W. Ordal, Diversity in chemotaxis mechanisms among the bacteria and archaea, *Microbiol. Mol. Biol. Rev.*, 2004, **68**(2), 301–319.
8 S. V. Plotnikov, A. M. Pasapera, B. Sabass and C. M. Waterman, Force fluctuations within focal adhesions mediate ECM-rigidity sensing to guide directed cell migration, *Cell*, 2012, **151**(7), 1513–1527.
9 R. Sunyer, V. Conte, J. Escribano, A. Elosegui-Artola, A. Labernadie, L. Valon, D. Navajas, J. M. García-Aznar, J. J. Munoz and P. Roca-Cusachs, Collective cell durotaxis emerges from long-range intercellular force transmission, *Science*, 2016, **353**(6304), 1157–1161.
10 E. Hadjipanayi, V. Mudera and R. A. Brown, Guiding cell migration in 3D: a collagen matrix with graded directional stiffness, *Cell Motil. Cytoskeleton*, 2009, **66**, 121–128.
11 S. B. Carter, Haptotaxis and the mechanism of cell motility, *Nature*, 1967, **213**(5073), 256.
12 P. P. Provenzano, D. R. Inman, K. W. Eliceiri, S. M. Trier and P. J. Keely, Contact guidance mediated three-dimensional cell migration is regulated by Rho/ROCK-dependent matrix reorganization, *Biophys. J.*, 2008, **95**(11), 5374–5384.
13 J. H. Wang and E. S. Grood, The strain magnitude and contact guidance determine orientation response of fibroblasts to cyclic substrate strains, *Connect. Tissue Res.*, 2000, **41**(1), 29–36.
14 P. P. Provenzano, D. R. Inman, K. W. Eliceiri, S. M. Trier and P. J. Keely, Contact guidance mediated three-dimensional cell migration is regulated by Rho/ROCK-dependent matrix reorganization, *Biophys. J.*, 2008, **95**, 5374–5384.
15 S. Wang and P. G. Wolynes, Active contractility in actomyosin networks, *Proc. Natl. Acad. Sci. U. S. A.*, 2012, **109**(17), 6446–6451.
16 T. Lecuit, P.-F. Lenne and E. Munro, Force generation, transmission, and integration during cell and tissue morphogenesis, *Annu. Rev. Cell Dev. Biol.*, 2011, **27**, 157–184.
17 C. A. Jones, M. Cibula, J. Feng, E. A. Krnacik, D. H. McIntyre, H. Levine and B. Sun, Micromechanics of cellularized biopolymer networks, *Proc. Natl. Acad. Sci. U. S. A.*, 2015, **112**(37), E5117–E5122.
18 S. B. Lindstrom, D. A. Vader, A. Kulachenko and D. A. Weitz, Biopolymer network geometries: characterization, regeneration, and elastic properties, *Phys. Rev. E: Stat., Nonlinear, Soft Matter Phys.*, 2010, **82**(5), 051905.

19 H. Mohammadi, P. D. Arora, C. A. Simmons, P. A. Janmey and C. A. McCulloch, Inelastic behaviour of collagen networks in cell-matrix interactions and mechanosensation, *J. R. Soc., Interface*, 2015, **12**(102), 20141074.
20 S. Nam, K. H. Hu, M. J. Butte and O. Chaudhuri, Strain-enhanced stress relaxation impacts nonlinear elasticity in collagen gels, *Proc. Natl. Acad. Sci. U. S. A.*, 2016, 201523906.
21 S. Nam, J. Lee, D. G. Brownfield and O. Chaudhuri, Viscoplasticity enables mechanical remodeling of matrix by cells, *Biophys. J.*, 2016, **111**(10), 2296–2308.
22 J. Kim, J. Feng, C. A. Jones, X. Mao, L. M. Sander, H. Levine and B. Sun, Stress-induced plasticity of dynamic collagen networks, *Nat. Commun.*, 2017, **8**(1), 842.
23 S. Chen, W. Xu, J. Kim, H. Nan, Y. Zheng, B. Sun and Y. Jiao, Novel Inverse Finite-Element Formulation for Reconstruction of Relative Local Stiffness in Heterogeneous Extra-cellular Matrix and Traction Forces on Active Cells, *Phys. Biol.*, 2019, **16**, 036002.
24 A. D. Doyle, N. Carvajal, A. Jin, K. Matsumoto and K. M. Yamada, Local 3D matrix microenvironment regulates cell migration through spatiotemporal dynamics of contractility-dependent adhesions, *Nat. Commun.*, 2015, **6**, 8720.
25 C. Heussinger and E. Frey, Force distributions and force chains in random stiff fiber networks, *Eur. Phys. J. E: Soft Matter Biol. Phys.*, 2007, **24**, 47–53.
26 F. Grinnell and W. M. Petroll, Cell motility and mechanics in three-dimensional collagen matrices, *Annu. Rev. Cell Dev. Biol.*, 2010, **26**, 335–361.
27 Y. L. Han, P. Ronceray, G. Xu, A. Malandrino, R. D. Kamm, M. Lenz, C. P. Broedersz and M. Guo, Cell contraction induces long-ranged stress stiffening in the extracellular matrix, *Proc. Natl. Acad. Sci. U. S. A.*, 2018, **115**, 4075–4080.
28 X. Ma, M. E. Schickel, M. D. Stevenson, A. L. Sarang-Sieminski, K. J. Gooch, S. N. Ghadiali and R. T. Hart, Fibers in the extracellular matrix enable long-range stress transmission between cells, *Biophys. J.*, 2013, **104**(7), 1410–1418.
29 P. Ronceray, C. P. Broedersz and M. Lenz, Fiber networks amplify active stress, *Proc. Natl. Acad. Sci. U. S. A.*, 2016, **113**(11), 2827–2832.
30 H. Wang, A. Abhilash, C. S. Chen, R. G. Wells and V. B. Shenoy, Long-range force transmission in fibrous matrices enabled by tension-driven alignment of fibers, *Biophys. J.*, 2014, **107**(11), 2592–2603.
31 F. Beroz, L. M. Jawerth, S. Münster, D. A. Weitz, C. P. Broedersz and N. S. Wingreen, Physical limits to biomechanical sensing in disordered fibre networks, *Nat. Commun.*, 2017, **8**, 16096.
32 L. Liang, C. Jones, S. Chen, B. Sun and Y. Jiao, Heterogeneous force network in 3D cellularized collagen networks, *Phys. Biol.*, 2016, **13**(6), 066001.
33 M. Dietrich, H. Le Roy, D. B. Bruckner, H. Engelke, R. Zantl, J. O. Radler and C. P. Broedersz, Guiding 3D cell migration in deformed synthetic hydrogel microstructures, *Soft Matter*, 2018, **14**, 2816.
34 G. Popkin, The Physics of Life, *Nature*, 2016, **529**, 16.
35 C. Bechinger, R. Di Leonardo, H. Lowen, C. Reichhardt, G. Volpe and G. Volpe, Active Particles in Complex and Crowded Environments, *Rev. Mod. Phys.*, 2016, **88**, 045006.
36 M. R. Nejada and A. Najafi, Chemotaxis mediated interactions can stabilize the hydrodynamic instabilities in active suspensions, *Soft Matter*, 2019, **15**, 3248–3255.
37 S. Torquato, T. M. Truskett and P. G. Debenedetti, Is Random Close Packing of Spheres Well Defined?, *Phys. Rev. Lett.*, 2000, **84**, 2064.
38 S. Torquato and Y. Jiao, Robust Algorithm to Generate a Diverse Class of Dense Disordered and Ordered Sphere Packings via Linear Programming, *Phys. Rev. E: Stat., Nonlinear, Soft Matter Phys.*, 2010, **82**, 061302.
39 H. Nan, L. Liang, G. Chen, L. Liu, R. Liu and Y. Jiao, Realizations of highly heterogeneous collagen networks via stochastic reconstruction for micromechanical analysis of tumor cell invasion, *Phys. Rev. E*, 2018, **97**(3), 033311.
40 C. Jones, L. Liang, D. Lin, Y. Jiao and B. Sun, The Spatial-Temporal Characteristics of Type I Collagen-Based Extracellular Matrix, *Soft Matter*, 2014, **10**, 8855.
41 D. A. Head, A. J. Levine and F. C. MacKintosh, Mechanical response of semiflexible networks to localized perturbations, *Phys. Rev. E: Stat., Nonlinear, Soft Matter Phys.*, 2005, **72**, 061914.
42 Y. Shokef and S. A. Safran, Scaling laws for the response of nonlinear elastic media with implications for cell mechanics, *Phys. Rev. Lett.*, 2012, **108**, 178103.
43 J. Steinwachs, C. Metzner and K. Skodzek, *et al.*, Three-dimensional force microscopy of cells in biopolymer networks, *Nat. Methods*, 2016, **13**, 171–176.
44 M. J. Powell, Site Percolation in Randomly Packed Spheres, *Phys. Rev. B: Condens. Matter Mater. Phys.*, 1979, **20**, 4194–4198.
45 L. Corte, P. Chaikin, J. P. Gollub and D. Pine, Random organization in periodically driven systems, *Nat. Phys.*, 2008, **4**, 420–424.
46 G. I. Menon and S. Ramaswamy, Universality class of the reversible-irreversible transition in sheared suspensions, *Phys. Rev. E: Stat., Nonlinear, Soft Matter Phys.*, 2009, **79**, 061108.
47 A. Franceschini, E. Filippidi, E. Guazzelli and D. J. Pine, Transverse alignment of fibers in a periodically sheared suspension: an absorbing phase transition with a slowly varying control parameter, *Phys. Rev. Lett.*, 2011, **107**, 250603.
48 I. Regev, J. Weber, C. Reichhardt, K. A. Dahmen and T. Lookman, Reversibility and criticality in amorphous solids, *Nat. Commun.*, 2015, **6**, 8805.
49 J. R. Royer and P. M. Chaikin, Precisely cyclic sand: Self-organization of periodically sheared frictional grains, *Proc. Natl. Acad. Sci. U. S. A.*, 2015, **112**, 49–53.
50 L. Milz and M. Schmiedeberg, Connecting the random organization transition and jamming within a unifying model system, *Phys. Rev. E: Stat., Nonlinear, Soft Matter Phys.*, 2013, **88**, 062308.
51 N. Mangan, C. Reichhardt and C. O. Reichhardt, Reversible to irreversible ow transition in periodically driven vortices, *Phys. Rev. Lett.*, 2008, **100**, 187002.
52 B. Brown, C. Reichhardt and C. Reichhardt, Reversible to irreversible transitions in periodically driven skyrmion systems, *New J. Phys.*, 2019, **21**, 013001.

53 Q.-L. Lei and R. Ni, Random-Organizing Hyperuniform Fluids with Momentum-Conserved Activations, arXiv:1904.07514, 2019.
54 W. Xu, X. Su and Y. Jiao, Continuum Percolation of Congruent Overlapping Spherocylinders, *Phys. Rev. E*, 2016, **94**, 032122.
55 M. Sahimi, Dynamic percolation and diffusion in disordered systems, *J. Phys. C: Solid State Phys.*, 1986, **19**, 1311.
56 S. Arbabi and M. Sahimi, Mechanics of disordered solids. I. Percolation on elastic networks with central forces, *Phys. Rev. B: Condens. Matter Mater. Phys.*, 1993, **47**, 695.
57 M. Sahimi and S. Arbabi, Mechanics of disordered solids. II. Percolation on elastic networks with bond-bending forces, *Phys. Rev. B: Condens. Matter Mater. Phys.*, 1993, **47**, 703.
58 X. Wang, R. Liu, S. Chen, H. Nan, Y. Ding, K. Song, J. Shuai, X. Zhang, Y. Zheng, F. Ye, Y. Jiao and L. Liu, Abnormal and rapid aggregation of invasive breast cancer cells induced by collective polarization and ECM mediated forces, 2019, submitted.